Infrared pyrometers for measuring dust explosion temperatures

K. L. Cashdollar, M. Hertzberg
Pittsburgh Research Center, Bureau of Mines, U.S. Department of the Interior
P.O. Box 18070, Pittsburgh, Pennsylvania 15236

Abstract

This paper will describe the design of two infrared optical pyrometers used to study dust explosions. One is a six-wavelength pyrometer that can measure both dust particle temperature and gas temperature by observing continuum and gas band emission in the 1 to 5 μm infrared region using PbSe detectors. The second pyrometer measures particle continuum emission in the 0.8 to 1.0 μm region of the near infrared using Si detectors. Temperature data are presented for both laboratory and full-scale mine explosions.

Introduction

There is a continuing interest in the accurate measurement of temperatures of dust explosions and fires. Most thermocouples have too slow a response time for observing explosions. Various optical methods have also been tried. However, temperature measurement based on the measured absolute radiance at a single wavelength is not applicable to situations where the dust flame is observed through an intervening cold dust cloud or a dust coating on the viewing window. Rapid scan spectrometers would provide measurement over a wide spectral region but may not be fast enough or rugged enough to observe some explosions.

This paper describes the design and use of two Bureau of Mines infrared (IR) pyrometers that can measure temperatures within full-scale mine explosions. Particle temperatures are calculated based on the best Planck curve fit of the measured continuum radiation at several wavelengths. Because only the relative radiation at each wavelength is used in the calculations, the attenuation of the flame radiation by a thin intervening cold dust cloud or a dust coating on the window does not affect the temperature measurement. One of the two pyrometers also measures the gas temperature in the explosion by observing the carbon dioxide emission band near 4.4 μm.

Pyrometer design

One Bureau of Mines pyrometer is a six-wavelength (6λ) instrument[1] that measures both particle and gas temperatures. This pyrometer was developed as an outgrowth of previous studies of laboratory-scale dust explosions using a rapid-scan infrared spectrometer.[2] An early model of the 6λ pyrometer is described in a prior publication.[3] The 6λ pyrometer uses lead selenide (PbSe) photoconductive detectors and infrared interference filters to measure flame radiation simultaneously at all six wavelengths. These wavelengths and their corresponding bandwidths are:

λ_1 = 1.57 μm	BW_1 = 0.16 μm
λ_2 = 2.30 μm	BW_2 = 0.10 μm
λ_3 = 3.84 μm	BW_3 = 0.16 μm
λ_4 = 4.42 μm	BW_4 = 0.17 μm
λ_5 = 4.57 μm	BW_5 = 0.19 μm
λ_6 = 5.00 μm	BW_6 = 0.26 μm

These effective wavelengths and full-width-at-half-maximum bandwidths were measured using the PbSe detectors. Figure 1 shows the positions of the six wavelengths on a graph of PbSe detectivity (based on manufacturer's data and corrected for the sapphire window transmission).

The explosion-proof version of the 6λ pyrometer used in the Bureau of Mines experimental mine is shown in Figure 2. Dust flame radiation enters through the sapphire window (3 mm thick and 64 mm clear aperture), and then an arsenic trisulfide lens (76 cm focal length) focuses the radiation on the filters and PbSe detectors located on the front face of the detector/amplifier box. The 4.8-degree viewfield of the pyrometer is virtually common for all of the six detectors if the dust flame is optically thick close to the window. Far from the window, the detector fields of view diverge at an angle of 1.9 degrees from the

center axis.

A smaller version of the 6λ pyrometer (Figure 3) is used to measure explosion temperatures in laboratory-scale flammability chambers. This model observes the flame through a sapphire window in the wall of the flammability chamber and therefore does not have to be explosion-proof. The detector/amplifier box on the left side of the figure contains the same detectors, filters, and amplifier circuits as in the mine version. However, a shorter focal length (36 cm) As_2S_3 lens is used, and the housing is more compact. An aperture over the lens limits the viewfield to 4.0 degrees for most observations instead of the full-aperture viewfield of 10.3 degrees. As with the mine version, the viewfields of all six detectors are virtually identical for flames that are optically thick close to the window. However, the viewfields diverge at a 4.0-degree angle far from the window.

A circuit diagram for two representative channels of the 6λ pyrometer is shown in Figure 4. All six channels have variations in the bridge resistors and amplifier gains to compensate for the differences in PbSe detectivity (Fig. 1) at the six wavelengths. Each bridge circuit is composed of two PbSe photoconductive detectors, two fixed resistors, and one variable resistor. Since the detectors operate at room temperature, their dark resistances vary with slight changes in ambient temperature. One of the PbSe detectors in each bridge is always dark and provides some temperature compensation for the other detector that views the flame radiation. Since the compensation is not perfect, the variable resistor in each bridge is used to set the zero radiation output voltage at the desired value. When a detector views infrared radiation, its resistance decreases and the resulting signal is amplified in two stages to provide an output voltage linearly proportional to the incident radiation. The intrinsic time response of the PbSe detectors is about 2 μsec, but the response of the pyrometer is limited to about 20 to 30 μsec due to the slower frequency response of the amplifiers. There is no need to chop the IR radiation at the detectors due to the short time duration of the dust explosions.

The second Bureau of Mines pyrometer is a three-wavelength (3λ) instrument that has been described in a previous publication.[4] A schematic diagram of the 3λ pyrometer is shown in Figure 5. Flame radiation enters through a quartz window and is split by two cube beamsplitters into three parts, each of which passes through an interference filter to a corresponding silicon photodiode. The three wavelengths are 0.80, 0.90, and 1.00 μm and the bandwidths are 0.01 μm each. The output of each photodiode is fed directly into an operational amplifier, thereby providing a linear output over several orders of magnitude of input radiation. The measured time response of the detector-filter combination ranges from 10 to 30 μsec for different versions of the pyrometer containing different amplifiers. A laboratory version of the 3λ pyrometer views explosions through a window in the flammability chamber. The three detectors in this version have identical fields of view of 4 degrees. An explosion-proof version (Fig. 5) of the 3λ pyrometer has been used to measure particle temperatures within full-scale mine explosions, and this version has identical viewfields of 8 degrees for each detector.

Planck radiation theory

The radiation emitted from an ideal blackbody is given by Planck's Law[5]:

$$M_\lambda = \frac{2\pi hc^2}{\lambda^5} [e^{hc/\lambda kT} - 1]^{-1}, \qquad (1)$$

where M_λ is the radiation emitted in energy per unit area per unit time per unit wavelength interval, h is Planck's constant, λ is the wavelength of the radiation, k is Boltzmann's constant, and T is the absolute temperature. For non-blackbodies,

$$H_\lambda = \varepsilon M_\lambda, \qquad (2)$$

where H_λ is the radiation emitted and ε is the emissivity. Since the voltage output from each channel of both the 3λ and 6λ pyrometers is linear with input radiation,

$$b_\lambda V_\lambda = a\varepsilon M_\lambda = \frac{2a\varepsilon\pi hc^2}{\lambda^5} [e^{hc/\lambda kT} - 1]^{-1} \qquad (3)$$

where V_λ is the voltage at one of the wavelengths, a is a constant scale factor independent of wavelength, and b_λ is a calibration factor for each wavelength. The constant, a, is a function of the fraction of the field of view of the pyrometer that is filled by the flame and the attenuation of the flame radiation by intervening, cold, unburned dust. The calibration factor, b_λ, is measured for each of the channels by calibrating each pyrometer with a standard blackbody cavity radiation source. The pyrometers were calibrated over the temperature range 1150 to 1450 K using a blackbody furnace (31 cm diameter spherical cavity with a 7.4 cm diameter viewing aperture). The linearity of the detectors allows the extra-

polation of this calibration to higher temperatures.

A cloud of burning dust particles emits continuum radiation according to Eq. (2). The emissitivity of a single particle is less than one and may vary with wavelength, but the combined emitted and scattered radiation from an optically thick cloud of dust particles produces an effective emissivity of close to one, independent of wavelength. Even for an optically thin cloud, the radiation should be gray (i.e. emissivity independent of wavelength) if the burning dust particles are significantly larger than the pyrometer wavelengths.

In addition to the particle continuum radiation from a carbonaceous dust explosion, there are also discrete emission bands from gases, especially water vapor and carbon dioxide. Figure 6 is an example of the gas band emission from a pure methane-air explosion (adapted from figure 1 in reference 2) at an optical path length of 25 to 30 cm-atm. For comparison, a 2000 K Planck curve at unit emissivity is shown. For optically thicker gas flames, the bands shown in the figure tend to increase in intensity, then broaden and extend to longer wavelengths. The positions of the six wavelengths of the 6λ pyrometer are also indicated. Notice that four of the wavelengths (1.57, 2.30 3.84, and 5.00 μm) were chosen to correspond to minima in the gas emission in order to observe the particle continuum radiation from a dust explosion. The other two wavelengths (4.42 and 4.57 μm) are at the strong CO_2 emission band and would measure gas radiation in addition to particle continuum radiation. For an optically thick flame that contains both hot particles and gases, the IR spectrum would be a continuum with superimposed emission or absorption bands depending on whether the gases are hotter or cooler than the particles.

For most of the observations with these two pyrometers, the dust cloud flame was optically thick and the emissivity was assumed to be gray for the temperature calculations. Therefore, in Eq. (3), the scale factor, a, can be combined with the emissivity, ε, into a single scale factor, aε, that is independent of wavelength. The relative radiation at each wavelength is the measured voltage multiplied by the blackbody calibration factor. For the particle temperature calculations, the measured, relative radiation at the dust continuum wavelengths is fitted by least squares to Eq. (3) to determine the two unknowns: the scale factor and the temperature. Note that the particle temperature calculations are made independently for the two pyrometers.

After the scale factor, aε, has been determined for the 6λ pyrometer, the gas temperatures can be calculated at 4.42 and 4.67 μm by assuming the same scale factor (i.e. gray emissivity) and using Eq. (3) and the measured radiation. This assumption of the same emissivity at the dust particle and gas wavelengths is only true for flames that are optically thick at the particle continuum wavelengths. Even for optically thick flames, there are complications because the two pyrometer channels, 4.42 and 4.57 μm, observe radiation from both the particles and the CO_2 gas. Because of the high emissivity per molecule of gas at 4.42 μm, the gas usually reaches unit emissivity over a shorter path length than the dust and therefore this channel would observe mainly gas radiation. At 4.57 μm, the gas has a lower emissivity per molecule and this pyrometer channel may reach unit emissivity for the gas and for the dust over a similar path length. This means that this channel would measure radiation from both the gas and dust and therefore measure a temperature that is some average of the gas and dust temperatures. An additional complication is that the gases in an explosion may cool as the flame front hits the window and the resulting self-absorption would reduce the measured gas radiation, especially at 4.42 μm. As a result of the above complications, the true gas temperature in the explosion is assumed to be the higher of the two temperatures calculated at 4.42 and 4.57 μm if the temperatures differ significantly.

Examples of the temperature calculations are shown in Figures 7 and 8, where the measured radiation, $b_\lambda V_\lambda/a\varepsilon$, is plotted versus the wavelength on a semi-logarithmic scale. Figure 7 shows the 6λ pyrometer data from a full-scale mine coal dust explosion. (This data was from an earlier version of the pyrometer in which the third wavelength was 3.46 μm rather than 3.84 μm.) The least squares fit of the four dust radiation data points to Eq. (3) is obtained by minimizing the squares of the deviations of the calculated scale factors at each wavelength from the average scale factor for the 4 data points; this is equivalent to minimizing the squares of the deviations of the logarithm of the radiation. The resulting calculated temperature is 1220 K with a standard deviation of 20 K. The calculated average gas temperature is 1410 K, but the possible self-absorption at 4.42 μm may mean that the true gas temperature is closer to the value of 1460 K calculated at 4.57 μm.

A second example of the temperature calculations is shown in Figure 8. For this data, the 3λ pyrometer and 6λ pyrometer simultaneously observed a coal dust explosion through a sapphire window in the top of an 8-liter flammability chamber[3]. For each pyrometer, the measured radiation, $b_\lambda V_\lambda$, is divided by the calculated average scale factor, aε, for that pyrometer and the combined data are plotted in the figure. The calculated particle temperature is 1830 K for the 6λ pyrometer and 1820 K for the 3λ pyrometer. The plotted Planck

continuum curve is for both temperatures. The calculated gas temperature measured from the excess radiation at the CO_2 band is 1990 K.

Not all of the data obtained with the 6λ pyrometer is as good as the data in Figures 7 and 8. For some confined dust explosions at high pressures, the 4.4 μm CO_2 gas band extends to longer wavelengths and even the 5.00 μm channel of the pyrometer may measure significant amounts of gas radiation in addition to particle radiation. In this case the particle temperature is calculated from the data from the first three channels of the pyrometer. For dust explosions that are optically thin at the dust wavelengths but still optically thick at the 4.4 μm CO_2 band, only the particle temperature can be calculated since the scale factors, $a\varepsilon$, would be different for the dust and for the gas.

Temperature data for dust explosions

Data obtained with the 6λ pyrometer for a full-scale mine explosion are shown in Figure 9. The nominal coal dust concentration was 200 mg/liter and it was inerted to 65% incombustible with added rock dust. The explosion was started at the closed face of the experimental mine and propagated toward the open end of the mine entry. A typical signal from one of the six channels of the pyrometer is shown in Figure 9A. The signal reached a peak near 1.5 sec as the main flame front passed the pyrometer, which was about 76 m from the mine face. The particle and gas temperatures calculated as a function of time are shown in Figure 9B. Note that the gas temperatures were several hundred degrees hotter than the dust particle temperatures and that the maximum difference coincided with the passage of the active flame front.

The two pyrometers have been used to simultaneously observe laboratory coal dust explosions in a closed 8-liter vessel. The details of the vessel and experimental procedure are found in reference 3. In brief, the dust was dispersed by a jet of air, and the resulting, uniform dust cloud was ignited. The two pyrometers viewed the flame radiation through a sapphire window in the top of the vessel. Temperature and pressure data as a function of dust concentration are shown in Figure 10 for a narrow size distribution of Pittsburgh seam coal dust with a surface mean diameter of 7 μm and a mass mean diameter of 9 μm. The pressure ratio curve in Figure 10B is the maximum explosion pressure divided by the initial pressure (approximately 1 atm). The temperatures shown were calculated at the time of maximum radiation for each explosion; this was slightly before the time of maximum pressure. The gas temperatures could not be calculated accurately below 300 mg/liter dust concentration because the dust becomes less optically thick and therefore has a lower emissivity than the 4.4 μm gas band. The maximum dust particle temperature and presumably the maximum gas temperature occur at a concentration of about 250 mg/liter, and this value is close to the concentration at which the burning velocity is a maximum for dusts in this size range[6]. It is also approximately the concentration at which the amount of combustible volatiles from the coal is at a stoichiometric ratio with respect to the air. The temperatures measured in this constant volume chamber are higher than those of atmospheric flames due to adiabatic compression. The gas temperatures for these explosions are from one hundred to several hundred degrees higher than the dust particle temperatures. This tends to confirm a combustion mechanism in which the coal particles devolatilize, generating hydrocarbon gases that combust in the gas phase. The dust particles remain cooler because of their continuing endothermic pyrolysis and the fact that the seat of the exothermic reaction is in the gas phase at a significant distance from the particle.

In Figure 10, the particle temperatures calculated from the two pyrometers generally agreed to within experimental error at the higher dust concentrations. At the lower dust concentrations (below 200 mg/liter), the temperature calculated from the 3λ pyrometer is significantly higher than that from the 6λ pyrometer. This is probably due to the fact that as the lean flammable limit concentration is approached, the flame becomes more filamentary and does not fill the entire chamber. This would result in a broad range of temperatures in the chamber, and the 3λ pyrometer would measure only the hottest particles because the radiation is a very steep function of temperature at wavelengths shorter than the Wien peak. At the longer wavelengths of the 6λ pyrometer, the radiation is not as steep a function of the temperature, and the pyrometer would observe more of an average temperature. For some dusts, the 3λ pyrometer measures a consistently higher particle temperature than the 6λ pyrometer even at high concentrations. This probably means a broad range of temperatures for these dust explosions. This effect has been observed for broad size distributions of coal dust containing some fairly large particles. It is reasonable that the smaller particles in such a dust would heat up to a higher temperature than the larger particles during the short timespan of the explosion.

Conclusion

The three-wavelength and six-wavelength pyrometers described in this paper are capable of measuring temperatures of dust explosions. The 3λ pyrometer is more compact and has no

zero drift for the detectors. It is therefore easier to use, but it measures only the dust particle continuum temperature in an explosion. The 6λ pyrometer is considerably larger and more complicated to use since the detectors must be rezeroed with changes in ambient temperature. It does, however, provide more information about a dust explosion by measuring both the particle and the gas temperatures. Both pyrometers are explosion-proof and have been used to measure temperatures within full-scale mine dust explosions.

References

1. Cashdollar, K. L., M. Hertzberg, and C. D. Litton (assigned to U.S. Department of the Interior). Multichannel Infrared Pyrometer, U.S. Patent 4,142,417, March 6, 1979.

2. Hertzberg, M., C. D. Litton, W. F. Donaldson, J. M. Kutchta, and A. L. Furno. Bureau of Mines Report of Investigations 7779, 38 pp., 1973.

3. Hertzberg, M., K. L. Cashdollar, and J. J. Opferman. Bureau of Mines Report of Investigations 8360, 70 pp., 1979.

4. Cashdollar, K. L., Applied Optics 18, 2595-2597, 1979.

5. Driscoll, W. G., Ed. Handbook of Optics (McGraw-Hill, New York, 1978), p. 1-13.

6. Smoot, L. D., M. D. Horton, and G. Williams. Sixteenth Symposium (International) on Combustion, The Combustion Institute, 1977, pp. 375-387.

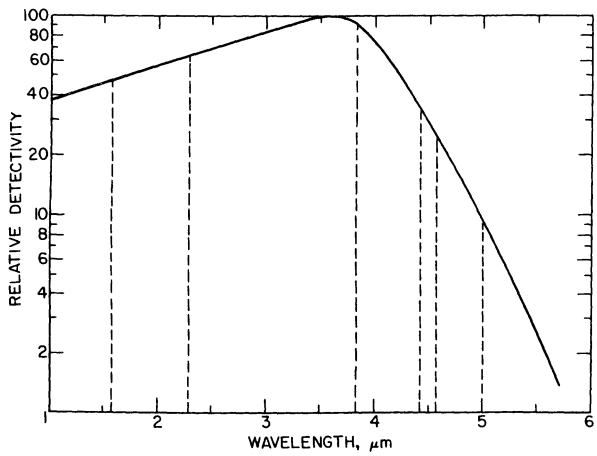

Figure 1. Lead selenide detectivity at the six pyrometer wavelengths.

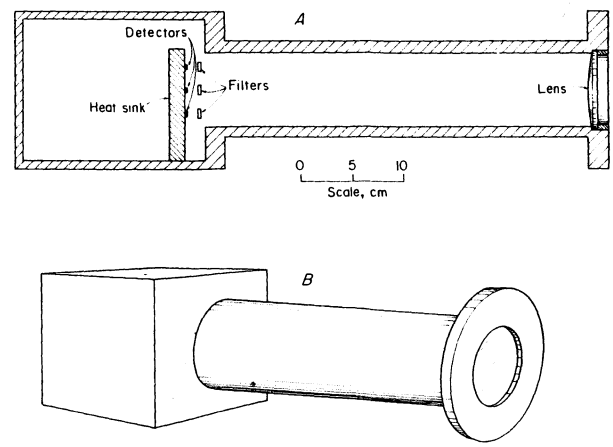

Figure 3. Laboratory version of the six-wavelength pyrometer.
A. Verticle cross-section showing internal components.
B. Perspective view.

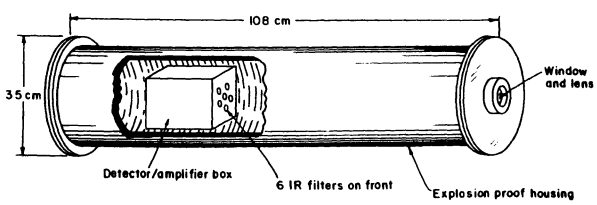

Figure 2. Mine version of the six-wavelength pyrometer.

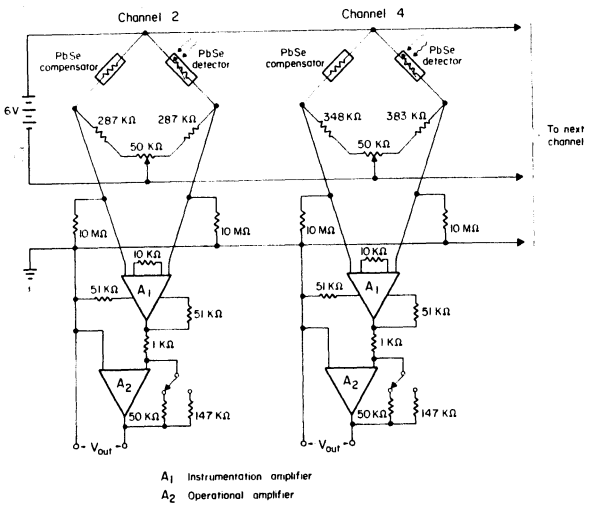

Figure 4. Circuit diagram for two channels of the six-wavelength pyrometer.

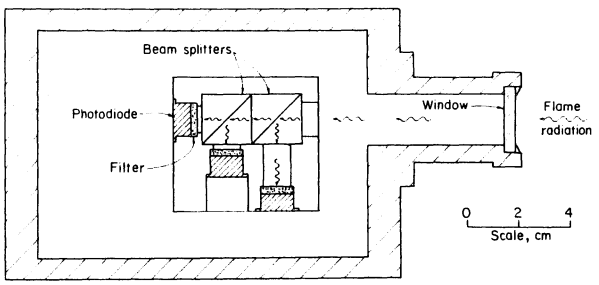

Figure 5. Mine version of the three-wavelength pyrometer.

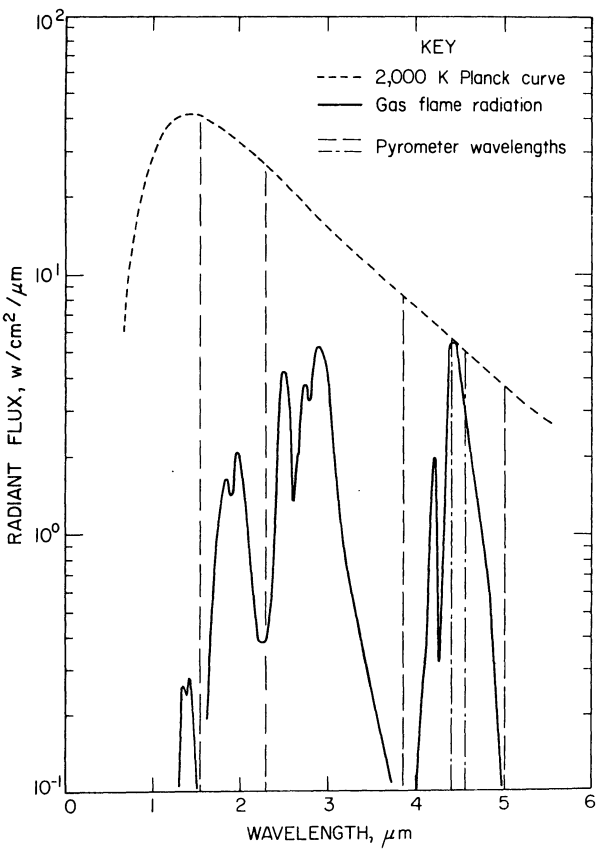

Figure 6. IR spectrum of a methane-air flame. Vertical dashed lines show the pyrometer wavelengths for comparison.

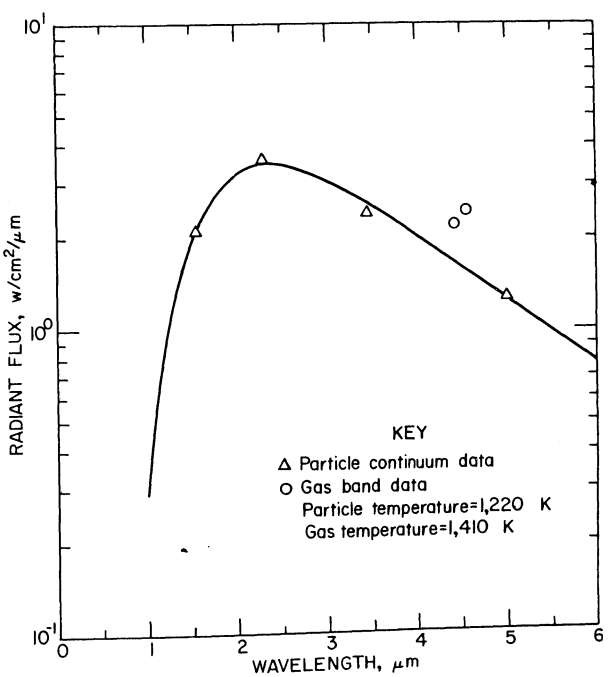

Figure 7. IR radiation from a coal dust explosion in the experimental mine, measured by the six-wavelength pyrometer.

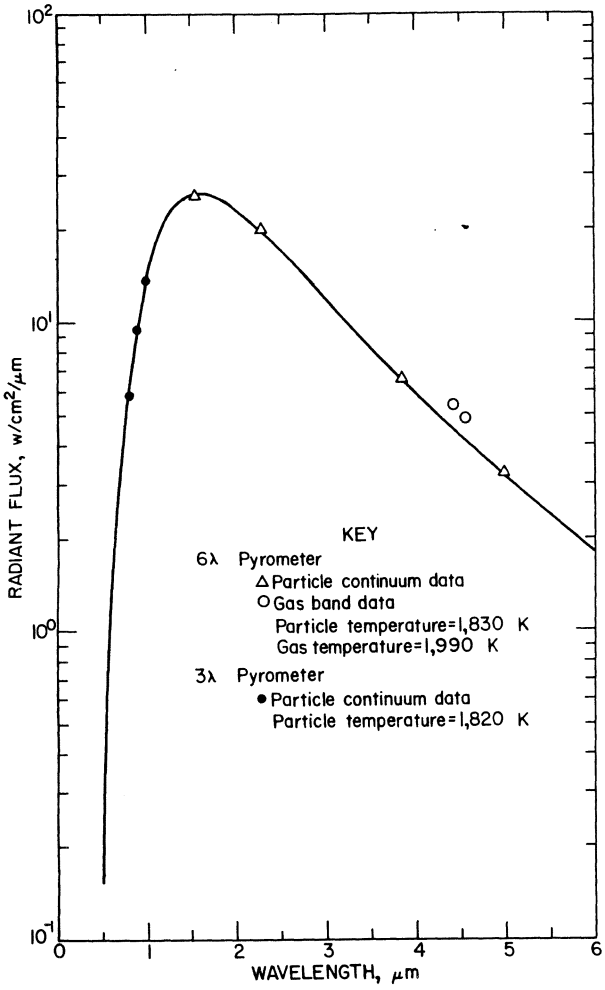

Figure 8. IR radiation from a coal dust explosion in a closed, 8-liter vessel, measured by the two pyrometers.

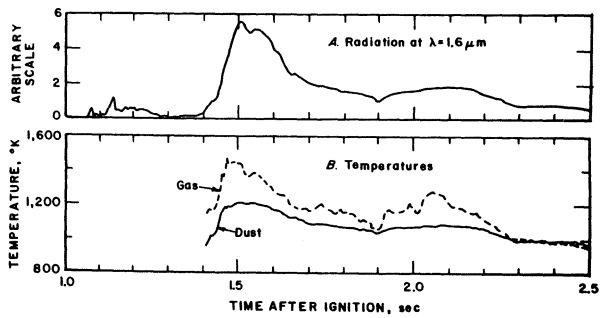

Figure 9. Observations of a full-scale mine explosion with the six-wavelength pyrometer.
A. Measured radiation at one wavelength.
B. Dust particle and gas temperatures.

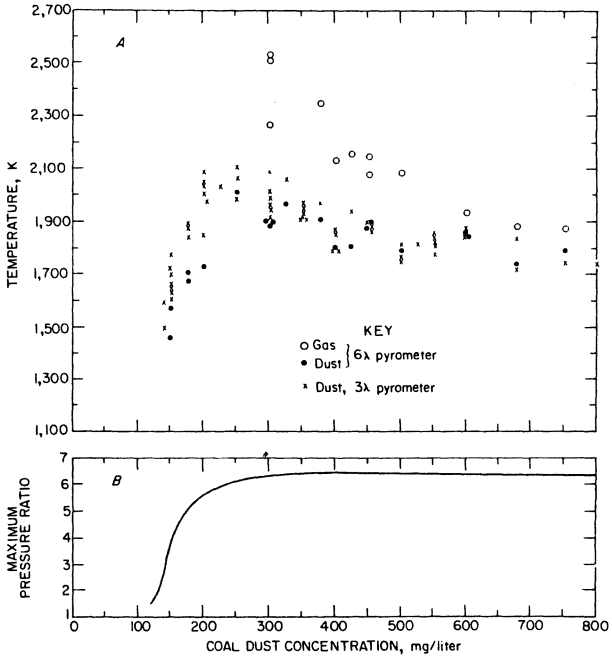

Figure 10. Observations of coal dust explosions in an 8-liter vessel.
A. Dust particle and gas temperature measurements with the two pyrometers.
B. Maximum explosion pressure ratio versus concentration.

Proceedings of the Society of Photo-Optical Instrumentation Engineers

Volume 253

Modern Utilization of Infrared Technology VI

Irving J. Spiro
Editor

July 31–August 1, 1980
San Diego, California

Published by
The Society of Photo-Optical Instrumentation Engineers
P.O. Box 10, Bellingham, Washington U.S.A. 98227
206/676-3290

The papers appearing in this book comprise the proceedings of the meeting mentioned on the cover and title page. They reflect the authors' opinions and have not been reviewed, refereed, edited, or copyedited. Their inclusion in this publication does not necessarily constitute endorsement by the editors or by the Society of Photo-Optical Instrumentation Engineers.

Please use the following format to cite material from this book:

Author(s), "Title of Paper," *Modern utilization of infrared technology VI,* Proc. Soc. Photo-Opt. Instr. Eng. 253, page numbers (1980).

Library of Congress Catalog Card No.: 80-52702

ISBN 0-89252-282-8

Printed in the United States of America.